

Application Note



ACT 5028 Resolver-To-Digital Converter

A Radiation-Hardened High-Precision Resolver-to-Digital Converter (RDC)

**by Nathan Nowlin & Steve McEndree
Microelectronics R&D Division ATK Mission Research**

**Daryl Butcher
Technology Applications Group**

Released with IEEE and Authors Permission

A Radiation-Hardened High-Precision Resolver-to-Digital Converter (RDC)

N. Nowlin, S. McEndree
Microelectronics R&D Division
ATK Mission Research
Albuquerque, NM

D. Butcher
Technology Applications Group
La Habra, CA

Abstract—We report for the first time radiation data on a radiation-hardened high-precision Resolver-to-Digital Converter (RDC). The RDC has a maximum of 16 bits precision, and is manufactured in a total-dose hardened $0.6\mu\text{m}$ CMOS process. Single-event (SEL) and dose-rate latchup hardening are designed-in using guard rings and DICE latches. Our results show total-dose hardness levels of $1\text{Mrad}(\text{SiO}_2)$, SEL and dose-rate latchup immunity, and geosynchronous-orbit single-event-upset (SEU) rates of 5×10^{-5} upsets/device/day.

Keywords—resolver, total dose, single event effects, dose rate, radiation hard, latchup, upset.

I. BACKGROUND

Resolver-to-digital converters (RDC's) are common system elements widely used to convert the analog sinusoidal outputs of resolvers (used for sensing angular shaft positions) to digital equivalents. Several commercial (non-rad-hard) RDC's are available, and they have been studied for their heavy-ion and dose-rate responses. In [1], Buchner, et al., studied the heavy ion responses of the Analog Devices AD2S80 16-bit RDC and the Data Device Corporation (DDC) RDC-19220 16-bit RDC. In [2], Mulford, et al., reported on the dose-rate response of the SDC-14616T (also manufactured by DDC). We report for the first time total-dose, heavy-ion, and dose-rate results on a rad-hard 16-bit RDC.

II. RDC OPERATION

Fig. 1 shows a typical architecture for a resolver-to-digital converter. Sinusoidal inputs of the form $\sin(\omega t)\sin(\theta)$ and $\sin(\omega t)\cos(\theta)$ are derived from an electromechanical resolver. The term $\sin(\omega t)$ is a carrier wave. The angle θ is the angle of the rotating shaft in the resolver relative to a fixed reference. These input sine waves are amplified and respectively multiplied by $\cos(\phi)$ and $\sin(\phi)$, where ϕ is an analog equivalent of the 16-bit output word in the data latch. A resistor network of sinusoidally varied values of resistance is used to convert the digital word to an analog voltage. The difference of the two transformed signals now represents an AC error signal, $\sin(\omega t)\sin(\theta - \phi)$. The error voltages AC1 and AC2 are derived from this signal. The carrier frequency component of the error voltages are filtered and demodulated then fed to an integrator. This generates a non-zero dc voltage when θ is not equal to ϕ . (Hysteresis is also built into the integrator.) As long as a non-zero input is being fed to the VCO, it is oscillating and driving an up-down counter that

increments or decrements the data latch to null the error voltage to zero. Once the error voltage is zero, the VCO shuts off, and the data in the data latch is a valid representation of the input angle. A busy pulse is toggled while the VCO is running to indicate the data latch is updating. The data latch can be inhibited through the use of the INH signal. The RDC is a mixed-signal, active-feedback system. As long as the device is not inhibited, it continuously corrects the output word when its analog equivalent differs from the input by more than the magnitude of the least significant bit (LSB).

III. RADIATION HARDENING METHODOLOGY

Total dose hardness was achieved by manufacturing our RDC in an Aeroflex $0.6\mu\text{m}$ radiation hardened process. [3] Our RDC design features a single 5V supply voltage in a 52-pin package. This technology allowed the design to be realized in a 53mm^2 die (Fig. 2). The architecture featured differential inputs and a ratiometric design. Our design operates on less than 150mW power, which is convenient for space system applications. Our RDC also allows for 16-, 14-, 12-, and 10-bit operation. The 16-bit mode offers the highest precision at the cost of tracking rate (only 16 rps, revolutions per second). The 10-bit mode allows higher tracking rates (1024 rps). In this paper, we will present results for the 16-bit mode of operation,

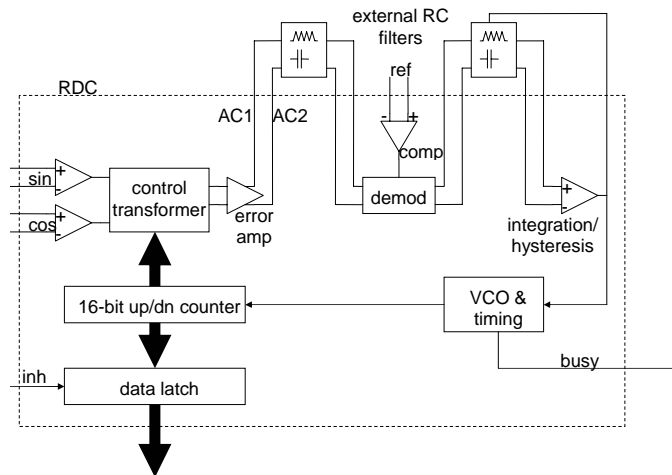


Figure 1. Block diagram showing elements of operation for a Resolver-to-Digital Converter (RDC).

This work has been funded through the Navy NAVSEA Crane under contracts N00164-97-D-0013 and N00164-02-D-6599.

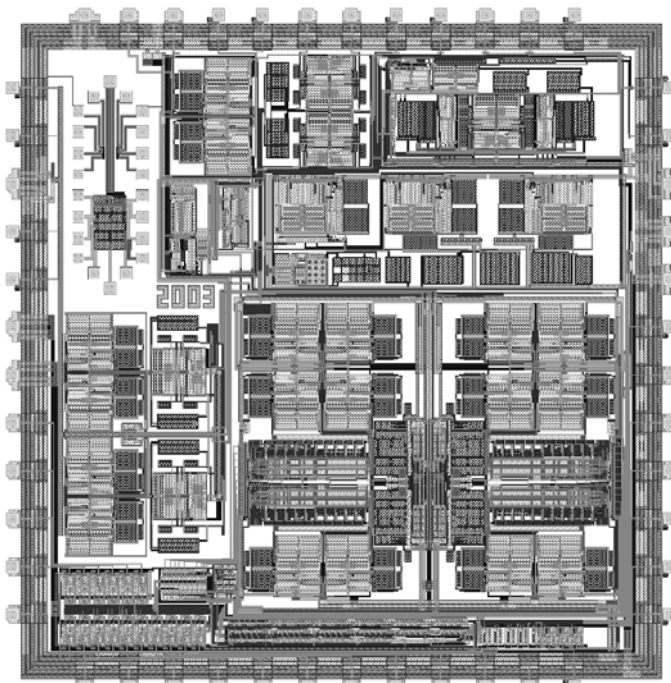


Figure 2. Layout of a radiation-hardened RDC.

as being the most sensitive mode for detecting small changes in performance.

Mitigation of single event effects was accomplished through the use of DICE latches in the digital output stages. [4] In addition, fully guard-banded layout techniques were used to provide substrate voltage control and minimize the possibility of latchup. This proved critical in achieving high dose-rate latchup immunity. An earlier design was found to be susceptible to dose-rate latchup at low dose rates ($\sim 10^{10}$ rad(Si)/s). Liquid-crystal thermal imaging was used to identify a large transistor pair in one of the amplifier drivers. There were too few guard ring contacts along the adjacent sides of the n+ and p+ guard rings around these transistors. This was fixed in a subsequent design modification by rerouting some of the metal. The design revision also included fixes to improve the output error (described below), various signal inversions, and lengthening some of the control pulse widths. Finally, because the RDC is a feedback control loop, upsets induced in the internal circuitry are automatically corrected.

In characterizing an RDC, and in particular the radiation response, we are most interested in the error between the output and the input angle. This is known as the integral non-linearity error, and is defined as the difference between the actual output word and the output word expected for the given input. In the 16-bit mode, the 360° input range is subdivided into 2^{16} steps. The output word 0001_{hex} is then $360/2^{16} = 0.0055^\circ$, or about $20''$ of arc. (This is the LSB, or least significant bit value.) This way, the output word can be converted to an angle in degrees and compared to the input angle in degrees. This difference, the INL, is plotted in Fig. 3 for several RDC's. Fig. 3 shows the INL error as a function of input angle for a commercial (non-rad-hard) AD2S80 (solid gray curve), our original RDC design (version 1, with the latchup problem noted above; gray dashes), our redesigned (version 2) RDC with a reduced

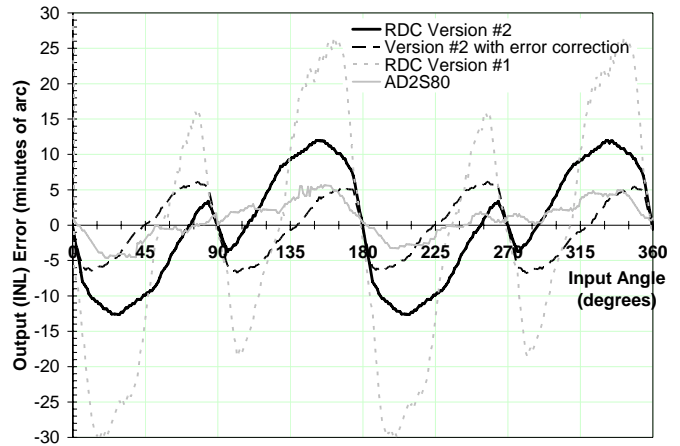


Figure 3. RDC Transfer Characteristic showing the output word error magnitude with each input angle for several RDC's.

magnitude INL (solid black curve), and the version 2 RDC with a simple error correction (dashed black curve). Note the clearly observable 20 and 40 degree periodicity to the error. The 20 degree harmonic distortion can easily be corrected in a system through a lookup table, or by introducing an offset between the sine and cosine input signals to trim out the error. Using a simple adjustment to the relative rms voltage offsets of the input signals, the corrected error of our RDC is nearly as good as the commercial AD2S80.

As we shall see, this INL error increases with total dose in non-rad-hard RDC's. In addition, single-event upsets manifest themselves as temporary changes in this INL error. In other words, heavy ions tend to induce temporary changes in the output word that are interpreted as new angles, differing from the input angle. As a result, the VCO turns on, generating a series of busy pulses while the feedback control loop of the RDC re-converges to the original INL error.

IV. TOTAL DOSE RESULTS

Two sets of total-dose tests were performed on our RDC designs. We tested version #1 of our RDC using the Low-Energy X-Ray (LEXR) facility at AFRL in Albuquerque, NM. Version #2 was tested with Co-60 gamma rays at the NAVSEA Crane, IN, Shepherd Irradiator. In both cases we had available both rad-hard and non-rad-hard versions of our RDC. (The non-rad-hard versions were obtained from process variants without the radiation hardened process modules.) Two parts (rad-hard and non-rad-hard) were tested with x-rays to several dose levels. Three parts of each process-split, rad-hard and non-rad-hard, were tested to gamma dose levels of 100 and 300 krad(SiO₂) respectively. Both experiments were performed with dose-rates of about 100rad(SiO₂)/s. The x-ray energy was 50keV. Each part was packaged in a 52-pin leadless chip carrier (LCC), and was exposed with the package lid removed. We followed up each set of radiation tests with 1-week, 100C anneals.

All non-rad-hard parts showed no degradation in performance to 100krad(SiO₂). Thereafter, one part ceased to

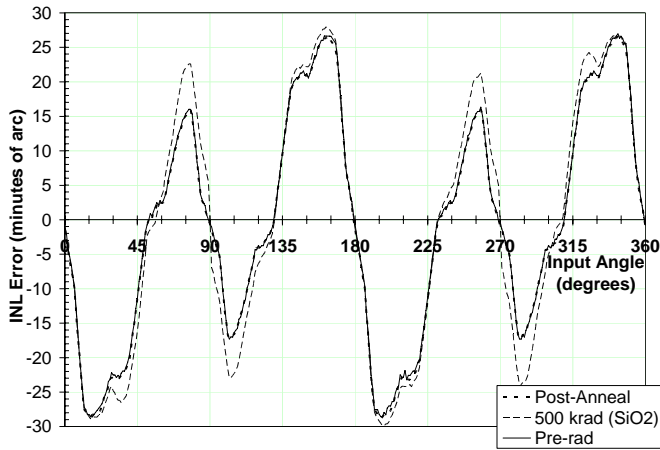


Figure 4. Typical INL Error vs. Input Angle for a non-rad-hard RDC at pre-rad, post-rad, and post-anneal levels.

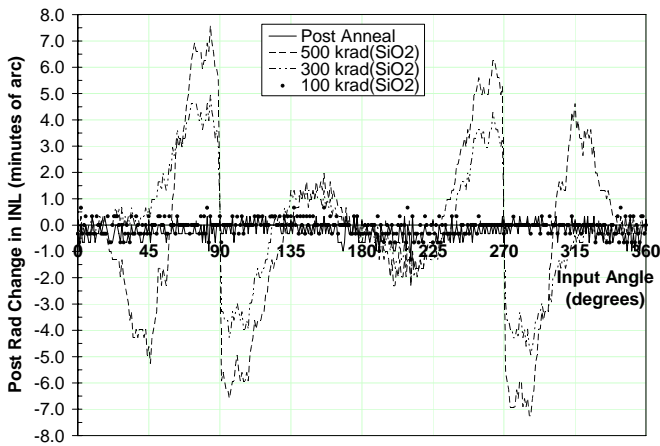


Figure 5. The difference of INL post-rad to INL pre-rad at each input angle for post-rad and post-anneal levels for a non-rad-hard RDC.

function (output did not change in response to input angle changes) and another began to show noticeable degradation in INL. Annealing restored functionality to the failed part, and reduced the INL error back to its pre-rad value. The non-rad-hard parts also showed slightly more increase in power supply current IDD than did the rad-hard parts. The rad-hard parts showed no loss of precision to total dose levels of 1.5Mrad(SiO₂), but one part ceased to function after a total dose of 2Mrad(SiO₂). Our measurements of the error voltage indirectly suggest the possibility of a failure in the bandgap circuit for this part. Annealing did not restore functionality.

Fig. 4 shows the INL error as a function of input angle for pre-rad, post 500 krad(SiO₂), and post-anneal levels. The overall magnitude of the INL increases very little (at the peaks around 15, 175, 195, and 345 degrees). However, the lesser peaks around 75, 105, 255, and 285 degrees increase noticeably. The point-by-point change in INL, INL post-rad minus INL pre-rad, is shown in Fig. 5 to emphasize the total dose effects seen at 300krad(SiO₂) and above. This represents an increase in INL of 20-30 bits, or about 20-30%.

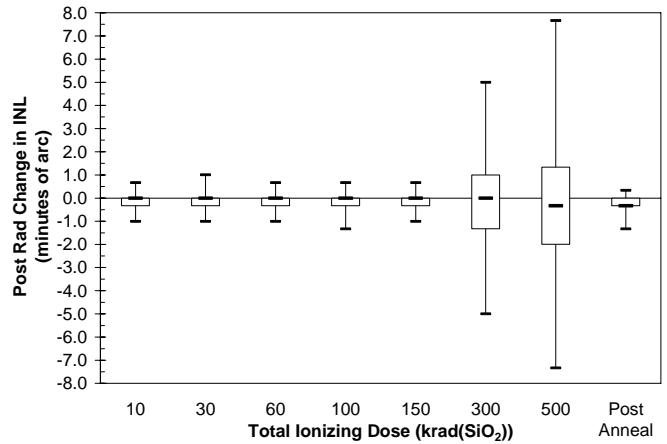


Figure 6. Box-plot distributions of post-rad changes in INL at each total dose level for a non-rad-hard RDC.

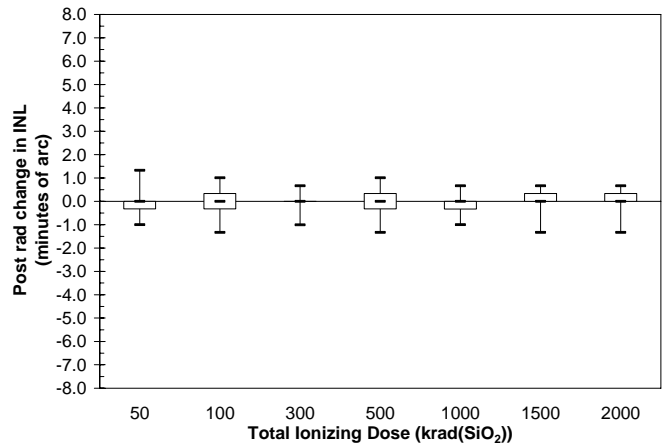


Figure 7. Box plot distributions of post-rad changes in INL at each total dose level for a rad-hard RDC.

For comparison to the total dose response of the rad-hard RDC's, we plot in Fig. 6 the data at each total dose level as a series of box plots. The increase in range of the INL error is clearly evident at 300 and 500 krad(SiO₂). In contrast, the same data for a rad-hard RDC, plotted in Fig. 7, shows no degradation of precision to total-dose levels over 1Mrad(SiO₂). In this test, the rad-hard part did fail after 2Mrad(SiO₂). Consequently, no post-anneal data were available. Note, however, that the non-rad-hard part (Fig. 6) fully recovered its pre-rad precision after a 1 week, 100C anneal.

We also measured the power supply current at each total dose stop in all our irradiation tests. Ionizing dose induces leakage paths in non-rad-hard CMOS transistors. We could therefore expect to see an increase in power supply current as more transistor leakage current flows with increasing total dose. This does appear to be the case, at least to a small degree, as seen in Fig. 8. Fig. 8 shows the relative increase in power supply current as a function of increasing total dose. Several data sets are shown. The solid curves, solid symbols show x-ray data. Open symbols and dashed curves show Co-60 data. The non-rad-hard parts, in gray, show a far more rapid rate of

increase in IDD with total dose. The one part that increased more than 25% failed to function, until annealing brought the value back under 25%. While in the Co-60 tests, at least, the rad-hard parts, in black, also showed significant increases in IDD (up to 20%), they remained functional at much higher total dose levels. The one rad-hard part that did lose functionality at 2Mrad(SiO₂) showed the lowest increase in IDD. This part likely failed for a mechanism other than CMOS leakage, as evidence from measurements of the error voltages AC1 and AC2 suggest.

These measurements are shown in Fig. 9. The post-rad changes in AC1 and AC2 relative to the pre-rad values for each chip are plotted vs. total dose. The squares show the AC1 values and the triangles show the AC2 values. Here, AC1 and AC2 are measured by disconnecting the RC filters (Fig. 1) and grounding all four inputs (\pm sine and \pm cosine). The difference in AC1 and AC2 is an average of offset voltages from several internal amplifiers centered around the mid-level voltage. This offers further evidence of internal leakage currents in the RDC, and is an indirect indication of the performance of an internal bandgap reference circuit. Measured this way, AC1 and AC2 should tend to track each other. Note that this is roughly the case, and the two parts that lost functionality show clear

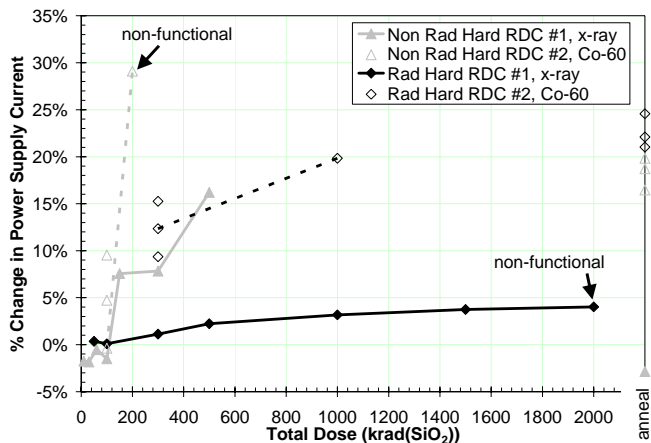


Figure 8. Increase in power supply current with increasing total dose.

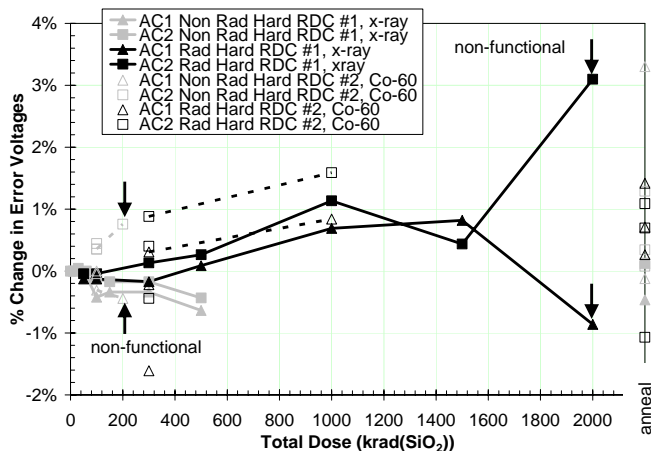


Figure 9. Post-rad changes in error voltages AC1 and AC2 for rad-hard and non-rad-hard RDC's tested in x-ray and Co-60 sources.

divergence at the point of loss of functionality. In fact, post-anneal measurements of the rad-hard part (tested to 2Mrad(SiO₂)) could not be made because the AC1 and AC2 values were drifting randomly.

V. SINGLE EVENT EFFECTS

Single-event-effects testing was done at Brookhaven National Laboratories' Tandem Van de Graaf accelerator facility. We exposed four rad-hard RDC's (version #2) to ion beams of gold, iodine, bromine, nickel, and chlorine with varying angles of incidence. Each part was packaged in a 52-pin leadless chip carrier (LCC), and was exposed with the package lid removed. The Aeroflex 0.6 μ m process is a three-level metal process with 5-7 μ m of metal and dielectric above the surface of the silicon. The ions lose some energy in traveling through these over-layers before depositing charge in the silicon pn junctions. We have therefore adjusted the linear energy transfer (LET) of each ion for its range at the silicon surface. The data used for these adjusted LET's can be found at [5]. Our adjusted LET_{eff} then accounts for the beam angle of incidence, α , both in the range (7 μ m \times sec(α)) and in the LET (adjusted LET \times sec(α)).

A. Single Event Latchup

We performed latchup testing with gold ions at a beam-incidence angle of 60° with our parts heated to 125C and biased at 5.5V. These are worst-case conditions for latchup testing. The input angle to the RDC was set to a constant rotation rate of 1° per second and the output and power supply currents were measured. Each part was exposed to a fluence of 10⁷ ions/cm². The details of these four beam runs are listed in Table I. Latchup was expected to be observed as a sudden large increase in power supply current during the beam run. However, the power supply current remained constant, and the part continued operating normally. No latchup was observed.

B. Single Event Upsets

We tested our RDC for upsets at room temperature and a power supply bias of 4.5V. These are worst-case conditions for heavy-ion-induced upsets. In purely digital systems, upsets are usually observed as changes in the logic state of control or memory bits during a static condition. We supplied a constant input angle of 120.000° to the RDC. As a result, the output word is expected to remain constant as well. An upset event will cause the output word to begin changing as the RDC first detects a difference in output angle and input angle. Then, through the action of the feedback control loop, the error is corrected in several output word steps. Thus, a single upset event might involve tens to thousands of output word changes. During a beam run, a computer continuously read the output word. Whenever an upset event occurred, the computer would detect the first output word change, increment an upset counter by 1, and then record the next 100ms of values from the RDC output word. (Our sample period was about 25 μ s.) The beam flux was adjusted to obtain an upset rate of about 1 upset per second. We ran the beam until we achieved at least 100 upsets or a total fluence of 10⁷ ions/cm², whichever came first. This allowed, in most cases, for the RDC to detect, respond to, and correct any upset errors induced by the beam before another

TABLE I. DATA FOR HEAVY-ION IRRADIATIONS.

Part	Ion	Beam		Incidence Angle degrees	Distance through overlayers	Adjusted LET	Adjusted LET _{eff}	Flux #/cm ² /sec	Fluence #/cm ²	Output Upsets	CrossSec cm ²	Comments
		Surface LET(Si) MeV-cm ² /mg	Maximum Overlayer Thickness									
LATCHUP TESTS												T=125C, VDD=5.5V
No.11	Au	84.00	7.00	60	14.00	55.80	111.60	3.70E+5	1.00E+7			no latchup
No.12	Au	84.00	7.00	60	14.00	55.80	111.60	2.44E+5	1.00E+7			no latchup
No.13	Au	84.00	7.00	60	14.00	55.80	111.60	3.65E+5	1.00E+7			no latchup
No.14	Au	84.00	7.00	60	14.00	55.80	111.60	2.18E+5	1.00E+7			no latchup
UPSET TESTS												T=25C, VDD=4.5V
No.13	Au	84.00	7.00	60	14.00	55.80	111.60	1.47E+3	5.44E+5	103	1.89E-4	16-bit mode testing
No.13	Au	84.00	7.00	60	14.00	55.80	111.60	2.05E+3	4.49E+5	105	2.34E-4	
No.13	lo	66.90	7.00	60	14.00	52.00	104.00	3.99E+3	4.85E+5	101	2.08E-4	
No.13	Au	84.00	7.00	45	9.90	66.00	93.34	5.25E+3	5.07E+5	100	1.97E-4	
No.12	lo	66.90	7.00	30	8.08	59.00	68.13	7.46E+3	8.43E+5	107	1.27E-4	
No.13	lo	66.90	7.00	0	7.00	60.90	60.90	9.03E+3	8.83E+5	102	1.16E-4	
No.11	Br	41.30	7.00	40	9.14	42.00	54.83	2.78E+4	1.36E+6	105	7.71E-5	
No.12	Br	41.30	7.00	30	8.08	42.00	48.50	2.50E+4	1.93E+6	111	5.76E-5	
No.12	Br	41.30	7.00	0	7.00	42.00	42.00	5.17E+4	2.11E+6	105	4.98E-5	
No.11	Ni	27.90	7.00	40	9.14	29.70	38.77	2.71E+4	2.32E+6	100	4.30E-5	
No.14	Ni	27.90	7.00	25	7.72	29.40	32.44	2.69E+4	2.38E+6	104	4.36E-5	
No.11	Ni	27.90	7.00	0	7.00	30.60	30.60	2.69E+4	2.42E+6	104	4.29E-5	
No.13	Cl	11.50	7.00	60	14.00	12.60	25.20	3.09E+4	9.61E+6	102	1.06E-5	
No.13	Cl	11.50	7.00	45	9.90	12.40	17.54	4.09E+4	1.00E+7	23	2.30E-6	
No.14	Cl	11.50	7.00	25	7.72	12.20	13.46	3.34E+4	9.45E+6	8	8.47E-7	
No.14	Cl	11.50	7.00	0	7.00	12.20	12.20	6.31E+4	1.01E+7	4	3.97E-7	
No.13	Au	84.00	7.00	60	14.00	55.80	111.60	3.06E+3	6.34E+5	100	1.58E-4	12-bit mode

upset occurred. In fewer than 1% of the events did multiple strikes occur during the 100ms record period. The data for the various runs are presented in Table I.

The record of a sample beam run is shown in Fig. 10. The RDC output angle (with a constant input angle of 120°) is plotted as a function of time during the beam run. Each group of points is a single 100ms record of an event. There was a wide variety of events recorded, both in magnitude and direction. Some upsets caused a negative excursion and others a positive excursion in the output angle. The larger events (off scale in the figure) showed both positive and negative excursions. Though there appears to be some grouping of events in the representation of Fig. 10, the upset rate remained approximately constant. This is confirmed when we plot the event number against the event time, as seen in Fig. 11.

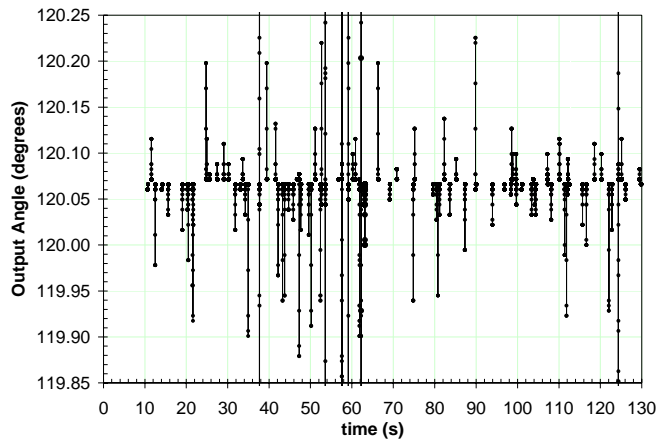


Figure 10. Record of upset events during a heavy-ion beam run.

To better understand the nature of these upsets, we plot in Fig. 12 and Fig. 13 a few examples of the two principal classes of upsets. First, in Fig. 12, we show a portion of the 100ms record of several events (on the same time scale) that are large-magnitude excursions (10's of degrees of angle). The overshoot response of these events is the consequence of the RDC feedback control loop correcting the error until convergence is reached. Note that the RDC converges back to the original output value within 50-60ms. (Lower resolution modes will converge more rapidly.) The direction and magnitude of these events is probably dependent on what circuit components are struck by the ion, but strikes in different circuits may yield similar responses, too. These large-magnitude strikes account for fewer than 10% of the events observed.

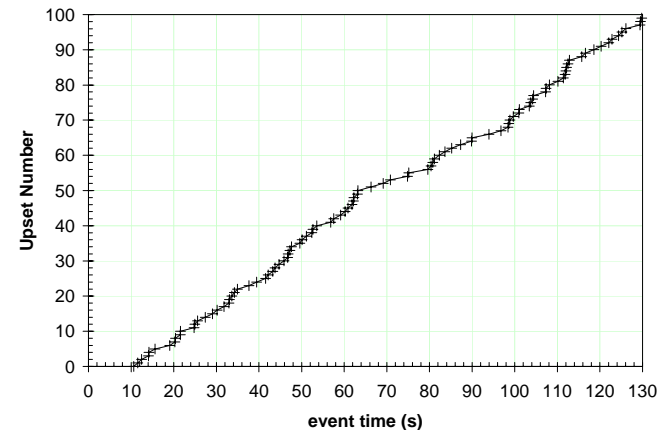


Figure 11. The number of upsets per second remained approximately constant throughout the beam run

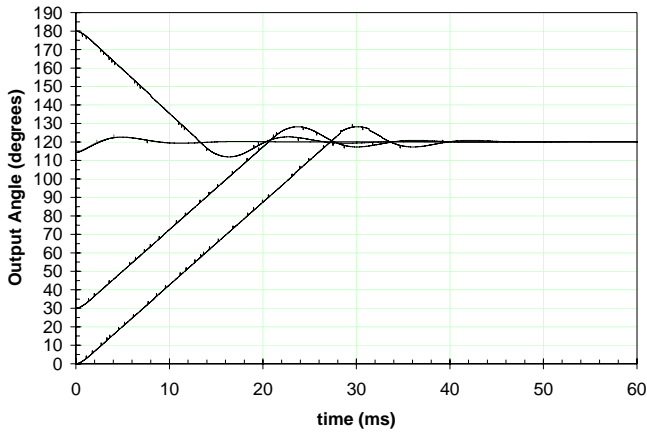


Figure 12. Examples of large-magnitude upsets with typical RDC feedback loop settling waveforms.

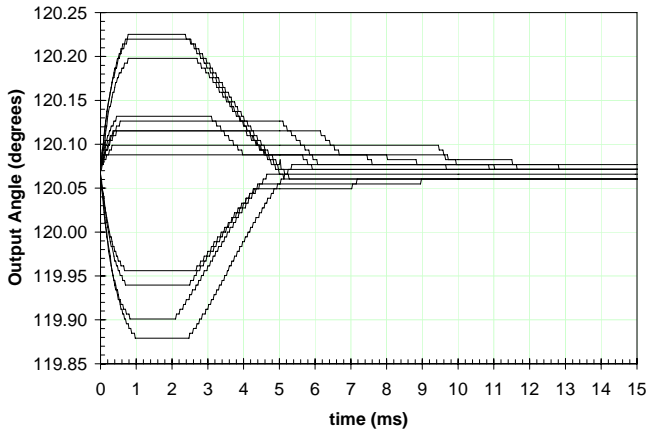


Figure 13. Examples of a few of the smaller-magnitude upsets with shorter durations.

(typically even smaller excursions) last perhaps 10 to 15ms. The vast majority of the events are of this type.

The full distribution of upset events can be better appreciated by plotting the magnitudes of all events (not just a few examples) on a normal distribution (or cumulative probability) graph. First we study the distributions at various time intervals within the 100ms record of each event. Fig. 14 plots on x the change (in digital counts) in output value relative to the starting (non-upset) value for each event against the normal standard deviation on y. (A normal distribution will plot as a straight line of slope equal to the standard deviation of the distribution on such a plot.) The various curves show the distributions of the recorded output values at 0ms (the first detected change), 1.2ms (where nearly all events have reached their maximum), 5ms (where a large majority of events have recovered), 15ms (where only the loop overshoots from larger events remain), 60ms (where all loop overshoots from larger events should be gone), and 100ms (the last data point, where the RDC output should have returned to its original value unless a secondary strike also occurred near the end of the record). We observe:

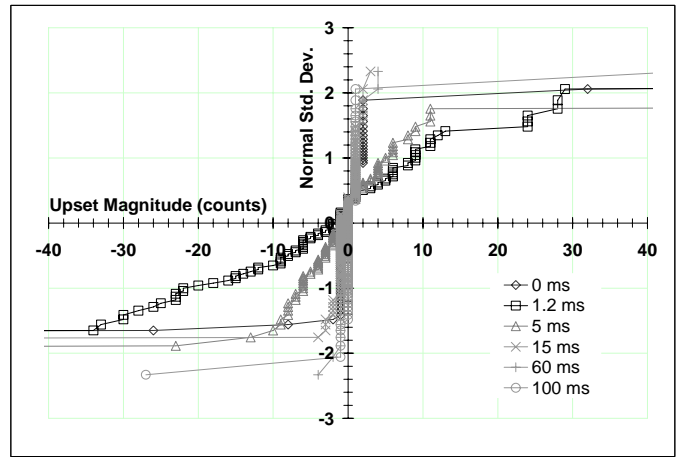


Figure 14. Normal distributions (cumulative probability) of upset magnitudes at various times during each 100ms record cycle.

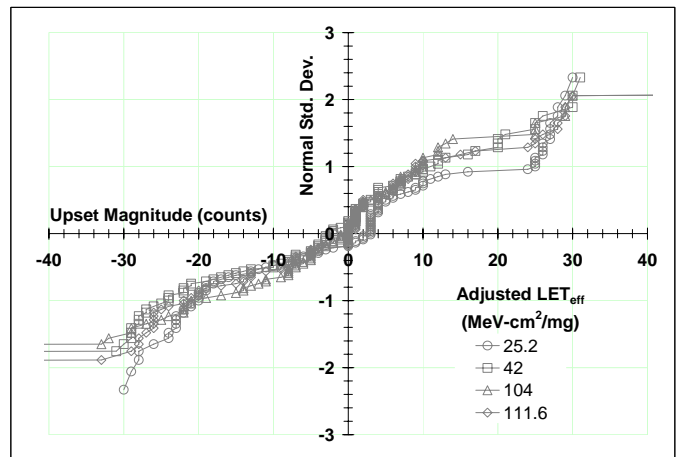


Figure 15. Normal distributions of peak upset magnitudes at several LET values.

(1) The first recorded output change (0ms curve) is almost always small in magnitude, only one or two bits. (2) Nearly all of the events have reached their peak magnitudes around 1.2ms. (3) The peak magnitudes typically range ± 30 counts with any value in this range nearly equally likely (due to the relatively small slope of the 1.2ms curve). (4) Most of the events are recovering or have recovered within 5ms (steeper slope of the 5ms curve). (5) After 15ms, only the small fraction of large loop overshoots remain, but (6) these are completely gone by 60ms (no tail on the distribution). (7) A few events (fewer than 1%) occur near the end of the 100ms run (tail on the 100ms curve), indicating an occasional case of multiple strikes within 100ms.

Our second study of the upset magnitude distributions is shown in Fig. 15, where the peak distributions at 1.5ms are plotted for several of the LET's in our experiment. We observe that the distribution of upset magnitudes is absolutely independent of LET for the small magnitude excursions! In contrast, the large magnitude excursions do disappear at the lower LET's (no tail on the 25.2 MeV-cm²/mg curve). It may

be possible to differentiate between these two types of upset events to identify either upsets in the digital circuitry or transients in the analog circuitry. However, further investigation using laser beams to isolate different regions of the chip would be required. [1]

Given this understanding of “upsets” in an RDC, we then follow the traditional analysis of calculating an upset cross section and estimating the error rate in a space environment. We do not calculate a bit upset rate, as one might for a memory, but rather we simply calculate a device upset rate. The upset data (cross-section vs. LET) of Table I are plotted in Fig. 16 for each of the ions and parts that we tested. The Weibull fit takes the following form,

$$1.8 \times 10^{-4} \text{ cm}^2 \left(1 - \exp \left[- \left(\frac{\text{LET} - 8}{52} \right)^{2.4} \right] \right)$$

where the LET is in MeV-cm²/mg, the saturation cross section is 1.8×10⁻⁴ cm², and the threshold is 8 MeV-cm²/mg.

The data above were used with CREME96 [6] to calculate upset rates. For these calculations, we assumed the worst-case geosynchronous orbit and 100 mils of Al shielding. We considered the flux of ions across the full range of atomic number (1 to 92) and assumed the RPP cross-section to be equivalent to the saturation cross-section of each error type considered. [7] Finally, we assumed a critical depth of 2μm. From these assumptions, we calculated an upset rate of 5.1×10⁻⁵ upsets/device/day for a device operated in the 16-bit mode.

For comparison, we also investigated the saturation of a device in the 12-bit mode. Analyses similar to the ones discussed in this section for the 16-bit data were also applied to the 12-bit data. The types and distributions of upsets were similar, as was the cross-section shown in Fig. 16. Such correlations suggest the upset rates for devices operated in lower-resolution modes should be about the same as those we measured in the 16-bit mode.

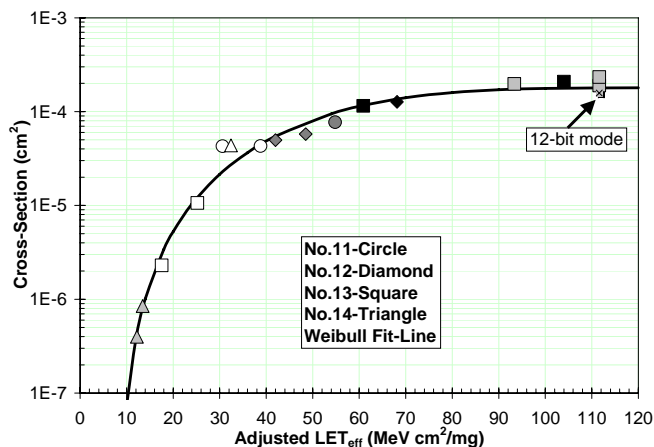


Figure 16. Upset cross-section vs. LET curve summarizing SEU results.

VI. DOSE-RATE LATCHUP RESULTS

Dose-rate testing was done in the linear accelerator (LINAC) at the NAVSEA Crane facility. The LINAC was configured for maximum dose rate and 20ns pulses. Dosimetry from thermo-luminescent dosimeters (TLD’s) was correlated to pin diode current pulses. This pin diode was placed directly in front of our test die to monitor the dose rate of each shot. We tested four version #2 rad-hard RDC’s with several shots each. This time, the parts were packaged in their flight-qualified CQFP packages. The lids were removed during LINAC testing. The RDC operating conditions were similar to those used for latchup testing in the heavy ion beam experiments: T=125C, VDD=5.5V, a fixed 120.000° input angle. We monitored IDD and the output data latch for evidence of latchup. The various runs are listed in Table II, showing the range of dose-rates achieved with the parts positioned as close to the beam aperture as possible. No latchup was observed at dose rates of 2×10¹¹ rad(Si)/s. Fig. 17 shows the photocurrent pulses measured on the pin diode (gray, right axis) and the RDC power supply line (ISS in black on the left axis). We see a 320mA pulse with a pulse width of about 300ns induced in the RDC.

The output response of the RDC was monitored for changes from the expected value of 120° in the same fashion as discussed above for the SEU testing. A typical example of the output response is plotted in Fig. 18. A large-magnitude loop settling waveform is observed as the RDC feedback loop corrects for the error and converges on 120° again within 40ms. Fig. 19 looks at the finer detail of the initiation of this excursion. Here we plot only the first millisecond of data. Because of the sampling rate of our computer, our first data point (at 0 μs) could have been detected at any time within 25μs of the LINAC pulse, and the second data point could have been as much as 50μs after the LINAC pulse. We observe that within this 50μs, the feedback control loop is fully functional, and the output angle begins to ramp linearly to re-converge on the expected 120° output angle. This is perhaps to be expected since the photocurrent pulse dissipates in less than 1/100th this time.

TABLE II. DOSE-RATES FOR EACH LATCHUP TEST RUN.

Run	Part	Dose Rate (rad(Si)/s)
31	466	1.80E+11
32	466	2.24E+11
33	466	2.20E+11
34	466	2.23E+11
35	466	2.17E+11
36	466	2.08E+11
94	465	2.07E+11
95	465	1.91E+11
96	465	2.10E+11
97	465	1.85E+11
122	467	1.82E+11
123	467	2.13E+11
124	467	2.01E+11
158	469	2.21E+11
159	469	2.14E+11
160	469	2.12E+11

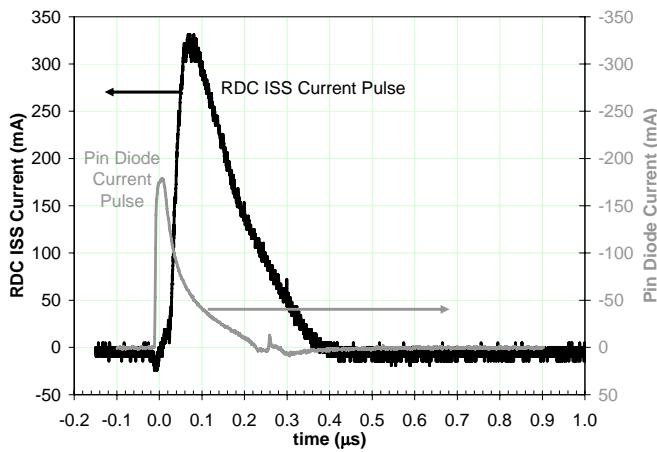


Figure 17. Typical dose-rate photocurrent pulses in the RDC and the pin diode used for dosimetry.

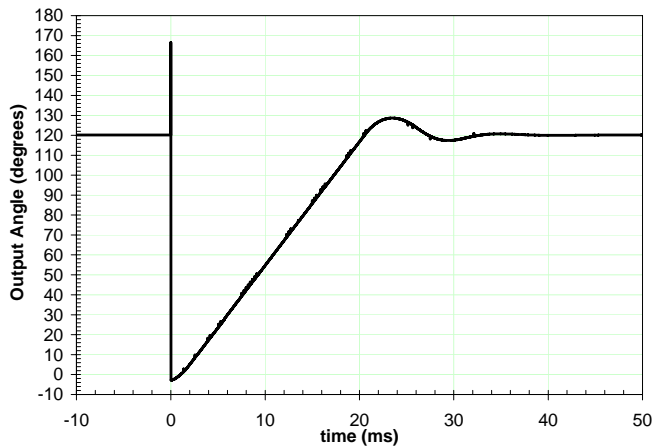


Figure 18. Typical photocurrent response of the RDC output.

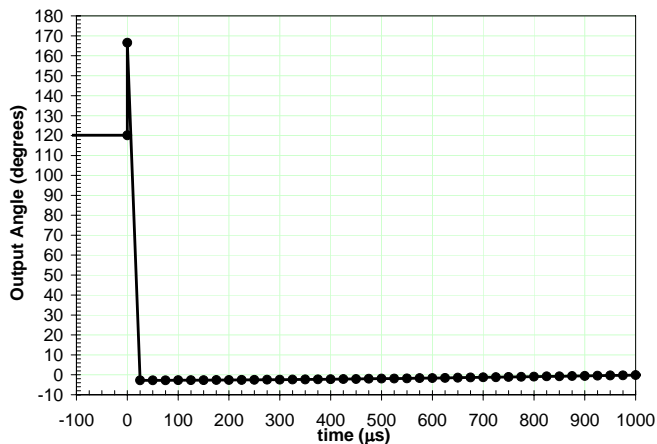


Figure 19. Typical photocurrent response of the RDC output (zoomed time scale).

VII. SUMMARY

We have successfully designed and manufactured a radiation-hardened high-precision Resolver-to-Digital converter. Our radiation test results show total dose hardness better than 1Mrad(SiO₂), SEL immunity to over 100 MeV-cm²/mg, an SEU threshold of 8 MeV-cm²/mg, and an SEU saturation cross section of 1.8×10⁻⁴ cm². A worst case heavy-ion upset rate is expected to be around 5×10⁻⁵ upsets/device/day. Our RDC is dose-rate latchup immune to over 2×10¹¹ rad(Si)/s.

ACKNOWLEDGMENTS

Our gratitude goes to Steve Clark of NAVSEA Crane for his continued interest in and support of this work. We also thank Joe Castaldo and Ron Sulyma of Aeroflex, Plainview, NY, and Danny Wilkin of Aeroflex, Colorado Springs, CO, for their contributions to the manufacture, qualification, and marketing of this product. Many thanks are due Marty Spanish of Technology Applications Group for layout and design support. Joe Benedetto of ATK Mission Research provided valuable heavy-ion test support, and we thank AFRL for the use of the LEXR facility.

REFERENCES

- [1] S. Buchner, L. Tran, J. Mann, T. Turflinger, D. McMorro, A. Campbell, and C. Dozier, "Single-Event Effects in Resolver-to-Digital Converters," *IEEE Trans. Nucl. Sci.*, Dec. 1999, pp. 1445-1452.
- [2] S. Mulford, D. Brown, A. McMaster, "Nuclear Dose Rate, Total Dose and Neutron Radiation Testing of COTS Devices," 2002 IEEE Radiation Effects Data Workshop, July 2002, pp. 145-151.
- [3] J.M. Benedetto, D.B. Kerwin, J. Chaffee, "Radiation Hardening of Commercial CMOS Processes Through Minimally Invasive Techniques," 1997 IEEE Radiation Effects Data Workshop, July 1997, pp. 105-109.
- [4] T. Calin, M. Nicolaidis, R. Velazco, "Upset Hardened Memory Design for Submicron CMOS Technology", *IEEE Trans. Nucl. Sci.*, Dec. 1996, pp. 2874-2878.
- [5] TVDG Ion Species, <http://tvdg10.phy.bnl.gov/species.html>.
- [6] A. Tylka, J. Adams, Jr., P. Boberg, B. Brownstein, W. Dietrich, E. Flueckiger, E. Petersen, M. Shea, D. Smart, and E. Smith, "CREME96: A Revision of the Cosmic Ray Effects on Micro-Electronics Code," *IEEE Trans. Nucl. Sci.*, Dec. 1997, pp. 2150-2160.
- [7] E. Petersen, J. Pickel, J. Adams, Jr., and E. Smith, "Rate Prediction for Single Event Effects—a Critique," *IEEE Trans. Nucl. Sci.*, Dec. 1992, pp. 1577-1599.

Aeroflex Plainview assumes no responsibility for the information contained in this application note, and no license or rights are granted by implication or otherwise in connection therewith.

Please visit our WEB site at www.aeroflex.com for the latest information.

Plainview Contact: Steve Friedman 516-752-2456

steve.friedman@eroflex.com

PLAINVIEW, NEW YORK

Toll Free: 800-THE-1553
Fax: 516-694-6715

INTERNATIONAL

Tel: 805-778-9229
Fax: 805-778-1980

NORTHEAST

Tel: 603-888-3975
Fax: 603-888-4585

SE AND MID-ATLANTIC

Tel: 321-951-4164
Fax: 321-951-4254

WEST COAST

Tel: 949-362-2260
Fax: 949-362-2266

CENTRAL

Tel: 719-594-8017
Fax: 719-594-8468

www.aeroflex.com info-ams@eroflex.com



As we are always seeking to improve our products, the information in this document gives only a general indication of the product capacity, performance and suitability, none of which shall form part of any contract. We reserve the right to make design changes without notice. All trademarks are acknowledged. Parent company Aeroflex, Inc. ©Aeroflex 2003.



Our passion for performance is defined by three attributes represented by these three icons: solution-minded, performance-driven and customer-focused